Physics of Fluids

Simultaneous impact of twin drops on a semi-infinite liquid target

Cite as: Phys. Fluids **33**, 102110 (2021); https://doi.org/10.1063/5.0067442
Submitted: 16 August 2021 . Accepted: 22 September 2021 . Published Online: 12 October 2021

Madison Artman-Breitung, Daren A. Watson and Andrew K. Dickerson

Physics of Fluids ARTICLE scitation.org/journal/phf

Simultaneous impact of twin drops on a semi-infinite liquid target

Cite as: Phys. Fluids 33, 102110 (2021); doi: 10.1063/5.0067442
Submitted: 16 August 2021 · Accepted: 22 September 2021 ·
Published Online: 12 October 2021

View Online Export Citation CrossMark

Madison Artman-Breitung,[1] Daren A. Watson,[2] and Andrew K. Dickerson[3,a)]

AFFILIATIONS

[1]Mechanical and Aerospace Engineering, University of Central Florida, Orlando, Florida 32816, USA
[2]Mechanical Engineering, Florida Polytechnic University, Lakeland, Florida 33805, USA
[3]Mechanical, Aerospace, and Biomedical Engineering, University of Tennessee, Knoxville, Tennessee 37996, USA

[a)]Author to whom correspondence should be addressed: dickerson@utk.edu

ABSTRACT

We take the enduring topic of drop impact on a deep pool of similar liquid further by allowing twin drops to impact simultaneously. Impacts are sufficiently proximal that impact crowns and craters interact, distorting and merging craters, and creating previously undocumented supersurface fluid interactions. The unique features of twin impacts occur when crowns collide to create a central veil that bifurcates the two craters and the expulsion of jet-like features atop colliding crowns. The emergence of a plethora of splash features is dependent on the Froude number ($\mathrm{Fr} = 30 - 200$) and drop separation distance. We analyze proximal crater evolution using theory developed for singular drops and develop scaling relations to predict crown and jet height. Crater and jet energies are compared for various impact velocities and drop separation distances. We find that craters close enough to merge produce thicker, but not higher, rebound jets.

I. INTRODUCTION

Despite the compendium of research focused on the impact of drops with solids[1–4] and liquid films,[5,6] studies focusing on the impact of drops on a deep pool are comparatively limited. The scarcity of deep pool impact studies is perhaps surprising due to the recent surge in liquid drop art and the ubiquity of raindrops falling on bodies of water. Nevertheless, studies of falling drops impacting deep pools have been given attention in relation to the underwater noise of rain,[7] rainfall impact on oil slicks,[8] and the physics of impact crater creation and collapse.[9,10] Drops impacting with sufficient gentleness, Weber number $\rho U^2 D/\sigma \lesssim 81$, where $\rho = 999\,\mathrm{kg/m^3}$ is the density of the fluid, U is the drop impact velocity, D is the drop diameter, and $\sigma = 72\,\mathrm{mN/m}$ is the surface tension, coalesce without crater formation,[11] but form a vortex ring that propagates downward into the pool. With sufficient impact velocity impacting drops create air-entraining cavities, or impact craters, on the floor of which the impact drop spreads, followed by the production of supersurface axisymmetric jets that may break up due to Rayleigh–Plateau instabilities.[11–17] At the free surface, a crown-like rim reaches skyward and may shed droplets if sufficiently thin. A short time later, the crater collapses. The physics of crater collapse is governed by impact conditions and may result in bubble entrainment, thick and thin central jets, and secondary drop formation.[11,18] Thin, fast jets are formed by capillary wave convergence, or pinching,[19] at the crater bottom, while thick, slower jets result primarily from surface tension and hydrostatic restoring forces. Bubble entrainment only occurs for thin, fast jets.[20] Collapsing craters form a vortex ring that propagates into the pool except for those entraining bubbles.[21] Weber–Froude (We–Fr) maps permit the prediction of the various jet and crater regimes,[11] where $\mathrm{Fr} = U^2/gD$ and $g = 9.81\ \mathrm{m/s^2}$ is the acceleration due to gravity.

In this experimental investigation, we film twin falling water drops impacting a liquid-free surface simultaneously and measure pertinent impact features. Drops impact close enough to one another such that their splash crowns, craters, and jets interact. We use four basic dimensionless groups to describe twin drop impact, the Reynolds number $\mathrm{Re} = \rho UD/\mu = 5950 - 15\,000$, the Froude number $\mathrm{Fr} = 30 - 200$, and a dimensionless spacing at impact $\ell^* = \ell/D = 1.2 - 5.1$. Drops impacting a distance ℓ from one another have diameter $D \approx 4.5$ mm, impact velocity $U = 1.2 - 2.9$ m/s, and viscosity $\mu = 0.89$ cP, fall under gravity g. Other studies have considered the impact of a liquid jet[22] and stream of drops,[23,24] which have the ability to generate deep and nested sub-craters. Our study is likely the first to film simultaneous, interacting impacts by drops side-by-side. The study perhaps most closely related to ours, Liu *et al.*[25] numerically studied the simultaneous impact of twin drops on a liquid film 10% the thickness of the drop diameter. The authors simulated

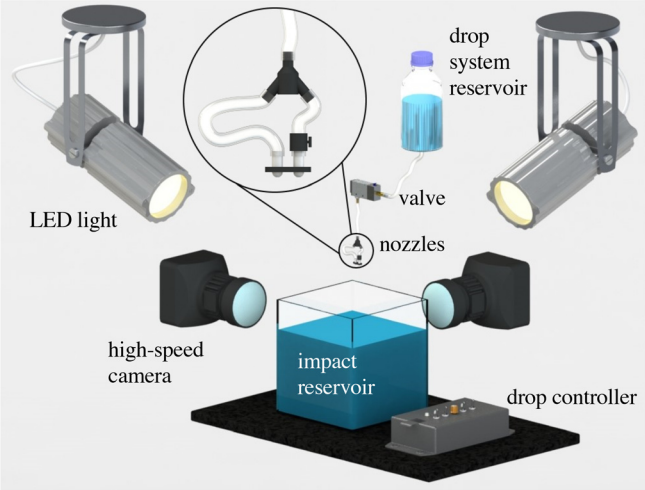

FIG. 1. Experimental setup.

the impact and splash of hollow drops and homogeneous drops, and found that hollow drops formed jets, whereas homogeneous drops formed only splash crown sheets. In both scenarios however, crown sheets collided to form a central liquid sheet, or veil, that collapses to form a central ring. We herein present similar features for experimental drops impacting a deep pool. We begin below by presenting our experimental methods in Sec. II and follow with a presentation of results in Sec. III. We discuss the implications of our results and directions for future work in Sec. IV.

II. EXPERIMENTAL METHODS

Drops are produced by the system schematized in Fig. 1. A water reservoir feeds a solenoid valve actuated by a HiViz AstroSplash Drop Controller. Valve timing is set to be open for approximately 36 ms, which produces two drops devoid of significant child droplets at pinch-off.[26] The valve output is split into two 3-mm-diameter nozzles nominally spaced $d = 5$, 15, and 21 mm apart depending on impact case. Impact cases are described by dimensional release parameters in the matrix of Table I. The tube leads to the two nozzles downstream of the splitter are of different lengths from one another such that one suffers a greater head loss. The shorter supply line is subsequently restricted with a manual, in-line ball valve that is adjusted such that two drops are emitted from the nozzles simultaneously. The adjustment of the system is done with trial and error. We measure left-hand drops, as shown in Fig. 3 (Multimedia view), have an average diameter $D = 4.67 \pm 0.28$ mm, N = 45, while right-hand drops average 4.38 ± 0.24 mm, N = 45. The global average diameter we use to define

TABLE I. Matrix denoting setup conditions for the nine impact cases.

		d (mm)		
		5	15	21
h (mm)	100	**1**	**2**	**3**
	200	**4**	**5**	**6**
	420	**7**	**8**	**9**

drop separation is 4.52 ± 0.30 mm, N = 90. The deviation in diameter between two drops in a pair ranges from 1.4 − 18.6% with an average of 6.8%. Nozzles are positioned at three heights $h = 10$, 20, and 42 cm on a ring stand. Impacts are illuminated by LED lights (GS Vitec MultiLED LT) and filmed with two synchronized high-speed cameras (Photron AX-200 and AX-100) at 5000 fps. The two cameras are set perpendicular to one another in the same plane to provide two orthogonal impact views. Drops fall into a rimless glass container measuring $20 \times 20 \times 20$ cm filled at least 5 cm deep. The liquid pool is emptied and replenished each day. Videos are analyzed with Open Source Physics Tracker (OSPT) and MATLAB. A circle fitter in OSPT is used to size impacting and secondary drops.

In our experiment, we are limited by nozzle size, and likely coalescence, in producing drops, which fall closer together. The reader will note that when $d = 5$ mm, $d/D = 1.1$. We show a typical drop release event in Fig. 2 (Multimedia view). Before pinch-off, drops grow in an elongated shape, far from contacting one another. At pinch-off, asynchronous oscillation ensures drops in Fig. 2 do not contact, but are separated by $< 200\,\mu$m at their closest point. Should oscillation become more synchronous, coalescence is possible. We thus posit our nozzles are at the lower limit of d to not produce coalescing drops. If drops do coalesce, this event is most likely to occur in the initial drop oscillation following pinch-off.

III. RESULTS

We perform impact trials of twin drops from three heights and three nozzle separation distances, with five replicates of each drop release condition for a total of 45 trials. Time sequence of all impact cases from a front view is shown in Fig. 3. Time sequences of impacts looking onto the free surface from a side view and at an elevated angle are provided in Fig. 4 (Multimedia view). A plot of ℓ^* vs Fr is shown in Fig. 5(a). Drops released from a greater height have more deviation in impact velocity U and drop spacing ℓ. We likewise observe drops migrate as they fall. We plot dimensional drop separation vs nozzle separation in Fig. 5(b), with ℓ and d labeled in the inset. For drops that are released very proximal ($d = 5$ mm), drops typically migrate away from one another. The cause for lateral drop migration is not well-

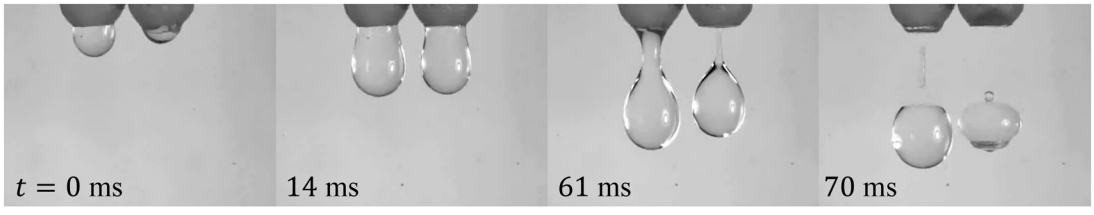

FIG. 2. Drops releasing from nozzles spaced such that $d/D = 1.1$. Multimedia view: https://doi.org/10.1063/5.0067442.1

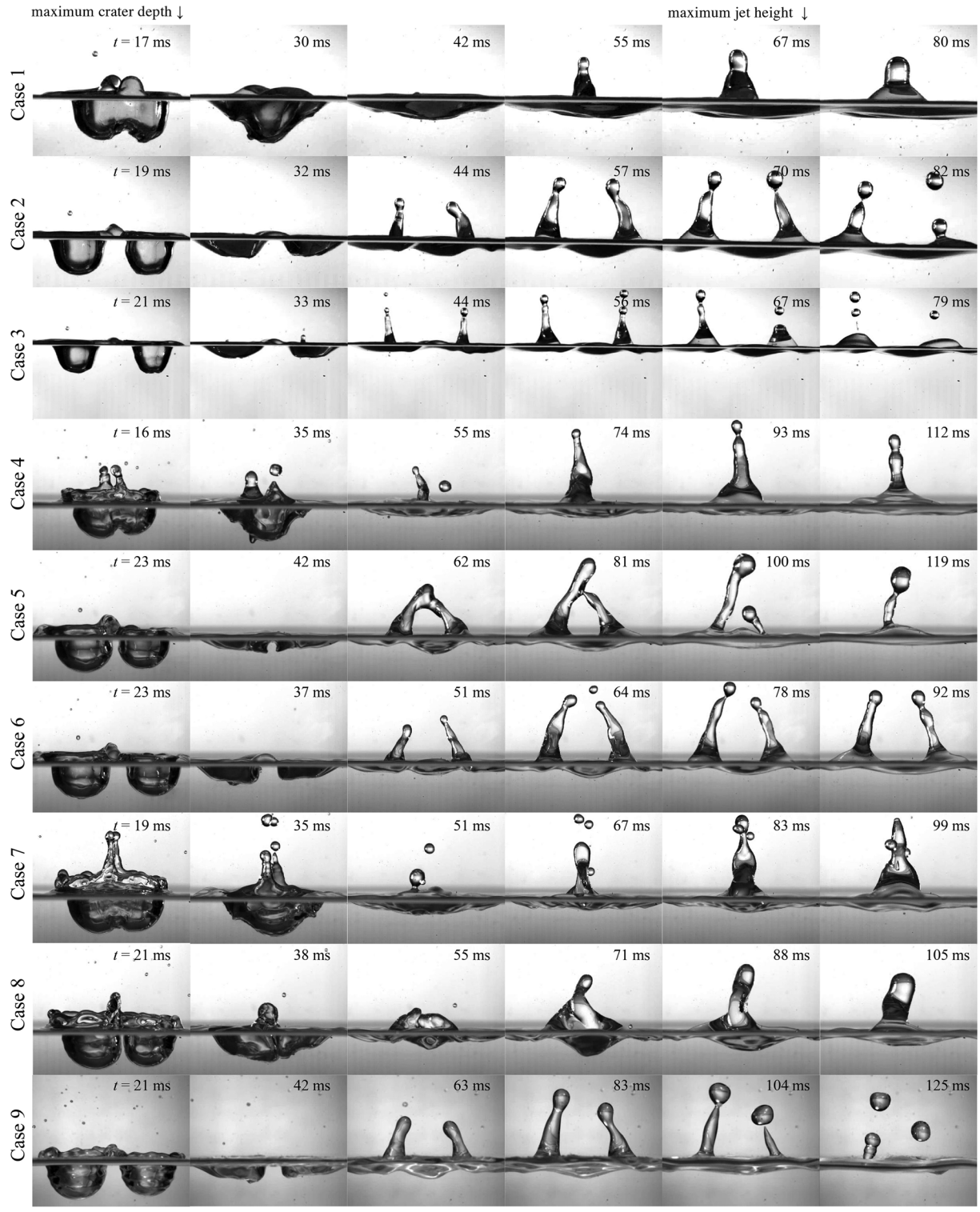

FIG. 3. Time sequences of impact. Left-most frames show the moment of maximum crater depth with $t = 0$ define as the moment drops contact the free surface. The fifth column from the left shows the moment of maximum coherent jet height. Intermediate and trailing columns are evenly spaced in time about cornerstone events. Multimedia view: https://doi.org/10.1063/5.0067442.2

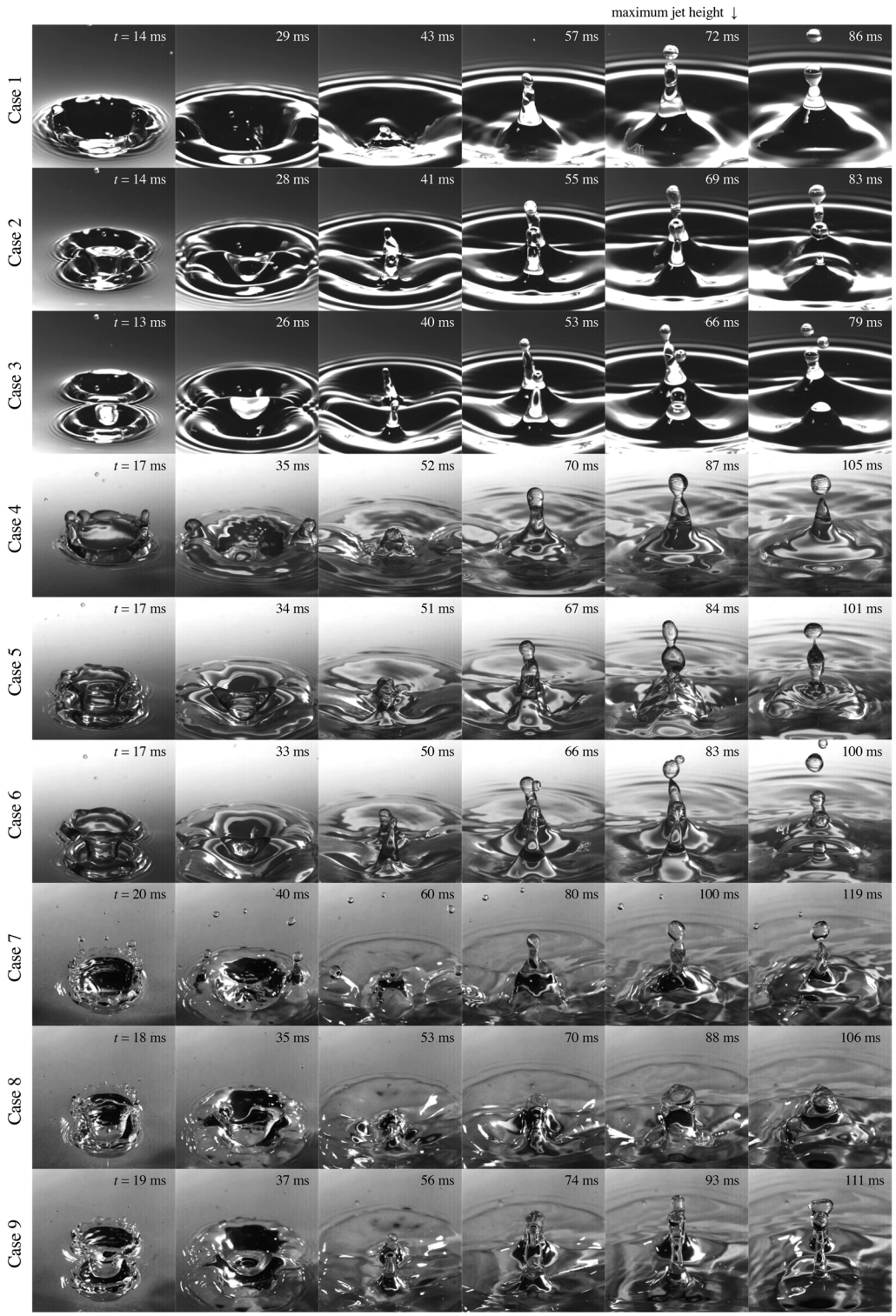

FIG. 4. Time sequences of impact looking onto the free surface from an angle of 30° with respect to the horizontal. The fifth column from the left shows the moment of maximum coherent jet height. Preceding frames show impact at 20, 40, 60, and 80% the time from first contact to jet maximum height, with the final columns at 120%. Multimedia view: https://doi.org/10.1063/5.0067442.3

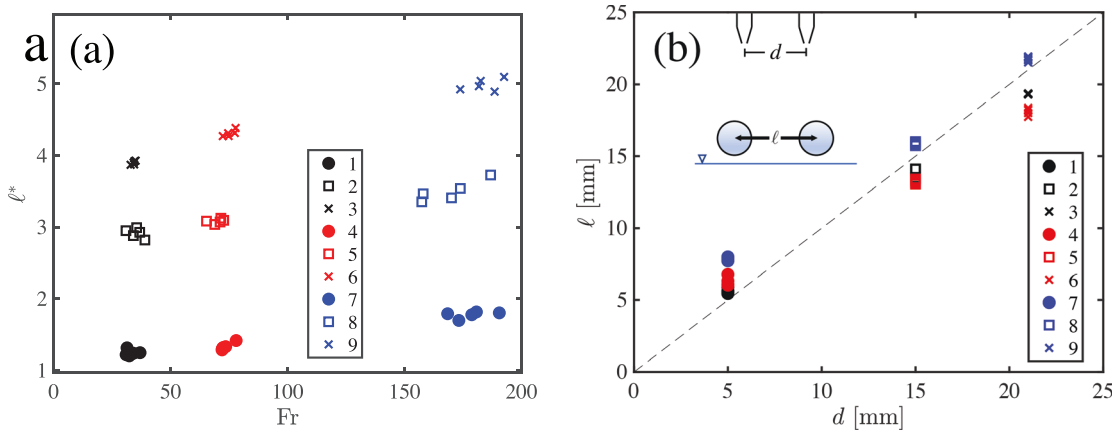

FIG. 5. (a) Non-dimensionalized drop spacing at impact ℓ^* vs Froude number. (b) Dimensional drop spacing at impact ℓ vs nozzle spacing d, with a line $\ell = d$ plotted for reference. The numbers in the legends refer to the impact cases described by Table I.

understood, but has been documented for spheres entering water side-by-side.[27] The flow of ambient fluid, air in our experiments, generates a high pressure region in the expanding wake. In contrast, drops that begin further from one another ($d = 15$, 21 mm) migrate toward each other for the two lowest drop heights. Thus, there may exist a lateral oscillation in the drops' paths as they fall, but such behavior remains uncharacterized.

A. Drop separation determines splash feature emergence

Both impact spacing and velocity govern the emergence of unique impact features throughout the splash progression, which is mapped in Fig. 6. We fix drop diameter at $D \approx 4.5$ mm and subsequently describe impacts by the dimensionless groups introduced in Sec. I, dimensionless crater depth Γ scaled by D, dimensionless crater width λ scaled by D, and dimensionless time τ scaled by D/U. For all impact trials where drops were closest ($\ell^* \approx 1.2 - 1.8$), cases 1, 4, and 7, splash crowns collide to form crown jets and a central veil between the two impact craters. The collapse of the central veil pushes the merged crater's free surface to a maximum depth. Further, veil collapse ushers the mating of two impact craters into a unified crater, which in turn retracts to form one central Worthington jet (Fig. 3). Breakup of the resulting central jet forms a secondary drop, which for case 7 is very large, measuring up to $1.7D$. We denote merging craters in all plots by using filled circles for data points. At the middle distance ($\ell^* \approx 2.8 - 3.7$), cases 2, 5, and 8, drop momentum promotes greater crater size and more jet interaction. In some cases, dual jets contact one another and coalesce. At the largest tested separation

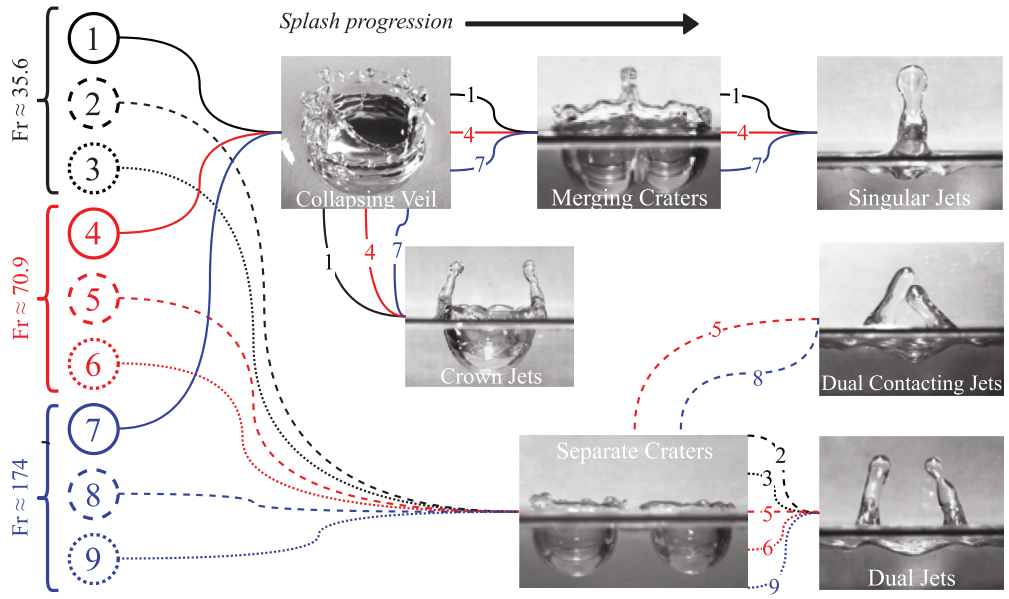

FIG. 6. Splash feature map.

($\ell^* \approx 3.9 - 5.1$), cases 3, 6, and 9, dual jets never contact one another but impact proximity promotes jets that eject at an angle biased toward one another. Above $\ell^* \approx 6.3$, impacting drops no longer appear to interact for the impact conditions tested.

From a side view of impacting drops, we can clearly measure the height of the splash crown h_c and the height of crown jets h_{cj}, for cases in which crown jets exist. We take the height of the crown to be that above the free surface of the tallest liquid point connected to the crown, for consistency. Our range of impact velocity produces crowns, which fit into three distinct regimes, qualitatively evidenced in the left-most column of Fig. 4. Cases 1–3 produce crowns only narrowly fitting the definition of a crown, and taking the form of gravity waves. The crowns of cases 4–6 are relatively thinner, taller, and with sparse spire formation. Cases 7–9 produce sheet-like ejecta with regular spires and rims dispelling a host of small droplets. While analytical expressions for crown evolution have been derived, no convenient scaling for crown height exists[6] to the authors' knowledge. We may however generate a justification for our observations by first asserting that the initial upward velocity of the crown rim $U_c \sim U$ and that the initial kinetic energy in the crown $\rho \mathcal{V}_c U_c^2/2$ scales with the crown's potential energy at its highest reach, $\rho \mathcal{V}_c g h_c$. Here, crown thickness can be neglected since crown volume $\mathcal{V}_c$ falls out of the scaling argument, $g h_c \sim U^2$, or equivalently,

$$h_c/D \sim \mathrm{Fr}. \tag{1}$$

We plot h_c/D vs Fr in Fig. 7(a) and note no obvious influence of drop spacing, which is expected because crowns grow before drop craters begin to interact. Despite the stark differences in crown morphology observed from the three drop heights, non-dimensional crown heights are well-described by Eq. (1) with a correlation factor $R^2 = 0.94$. A best fit yields $h_c/D \sim \mathrm{Fr}^{0.83}$ ($R^2 = 0.96$).

The colliding crowns of two adjacent drops form jet-like structures pictured in the sequences of Fig. 8 (Multimedia view). We dub this pair of jets "crown jets," witnessed only for cases 1, 4, and 7 (Fig. 6). At early impact times, these two crown jets are connected by a central liquid veil that bifurcates the two impact craters. Colliding splash crowns push this veil upward, thinning the sheet with respect to its parent splash crowns. The veil rapidly collapses, leaving the two crown jets that often break, forming secondary drops. The veil is analogous to the thin lamella formed when drops impact solid surfaces.[1] From the view pictured in Fig. 8, we measure coherent crown jet height h_{cj}, which is plotted against crown height h_c in Fig. 7(b). On average, crown jets are 2.8× higher than the crowns from which they are formed, and nearly proportional in height, $h_{cj} \sim h_c^{1.09}$ ($R^2 = 0.94$). Thus, from Eq. (1) and the experimental scaling of Fig. 7(b) we can write,

$$h_{cj}/D \sim \mathrm{Fr}. \tag{2}$$

A best fit yields $h_{cj}/D \sim \mathrm{Fr}^{0.99}$ ($R^2 = 0.96$) and is plotted in Fig. 7(c). While our simple scaling does well to predict crown and crown jet height, a more exact physical characterization of crown height for impacts into a deep pool is an area for future research.

B. Proximal craters constrain fluid flow

We use image subtraction[2,28] to acquire spatiotemporal traces of craters from consecutive frames as shown by crater traces in Fig. 9. Crater evolution is captured every $\Delta t = 200\ \mu$s. The influence of drop impact proximity on crater expansion is apparent when one compares the red and black traces to that of a green single drop impact in Fig. 9. Craters arising from impact cases with minimal drop separation $d = 5$ mm [i.e., cases 1—Fig. 9(a), 4—Fig. 9(b), and 7—Fig. 9(c)] are constrained radially during expansion, resulting in increased curvature of contacting regions and stymied crater growth. In the context of Mansoor *et al.*,[29] adjacent craters experience a "wall effect." For all other cases $d = 15$ and 21 mm, crater expansion is nearly unabridged and compares well with single drop impacts.

To further characterize the evolution of crater depth Γ, we employ a dimensionless model developed by Bisighini *et al.*[10] that assumes a crater of spherical curvature with dimensionless radius α and sphere centroid location ζ

$$\ddot{\alpha} = -\frac{3}{2}\frac{\dot{\alpha}^2}{\alpha} - \frac{2}{\alpha^2 \mathrm{We}} - \frac{1}{\mathrm{Fr}}\frac{\zeta}{\alpha} + \frac{7}{4}\frac{\dot{\zeta}^2}{\alpha} - \frac{4\dot{\alpha}}{\alpha^2 \mathrm{Re}}, \tag{3}$$

$$\ddot{\zeta} = -3\frac{\dot{\alpha}\dot{\zeta}}{\alpha} - \frac{9}{2}\frac{\dot{\zeta}^2}{\alpha} - \frac{2}{\mathrm{Fr}} - \frac{12\dot{\zeta}}{\alpha^2 \mathrm{Re}}. \tag{4}$$

Dimensionless crater depth $\Gamma = \alpha + \zeta$. For $\tau = Ut/D < 2$, crater depth growth is taken to be linear, such that

$$\dot{\alpha} \approx 0.17, \quad \alpha \approx \alpha_0 + 0.17\tau, \quad \dot{\zeta} \approx 0.36, \quad \zeta \approx -\alpha_0 + 0.36\tau, \tag{5}$$

where $\alpha_0 = 0.77$ is a constant related to initial crater radius.[10] Initial conditions are largely unchanged from the results of Bisighini *et al.*[10] except for $\dot{\zeta} \approx 0.36$, originally[10] employed as $\dot{\zeta} \approx 0.27$. Our chosen value of $\dot{\zeta}$ ensures an average best-fit correlation value $R^2 = 0.99$ for $\tau \leq 2$ across all impact cases. Equations (3) and (4) are solved with

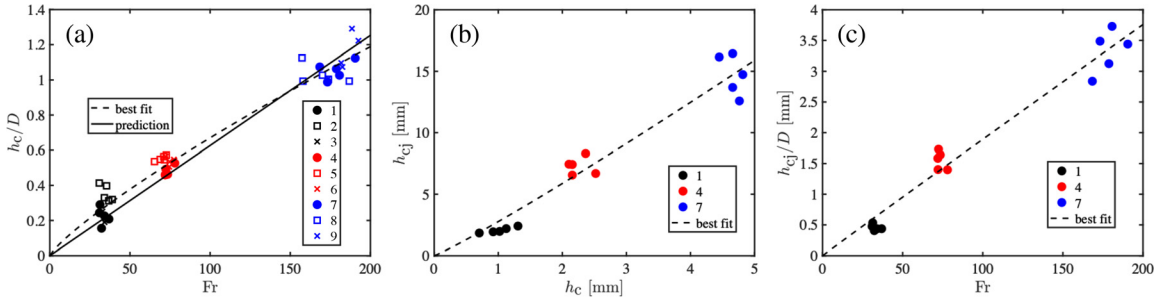

FIG. 7. (a) Non-dimensionalized crown height vs Froude number. (b) Crown jet height h_{cj} vs crown height h_c. (c) Non-dimensionalized crown jet height vs Froude number.

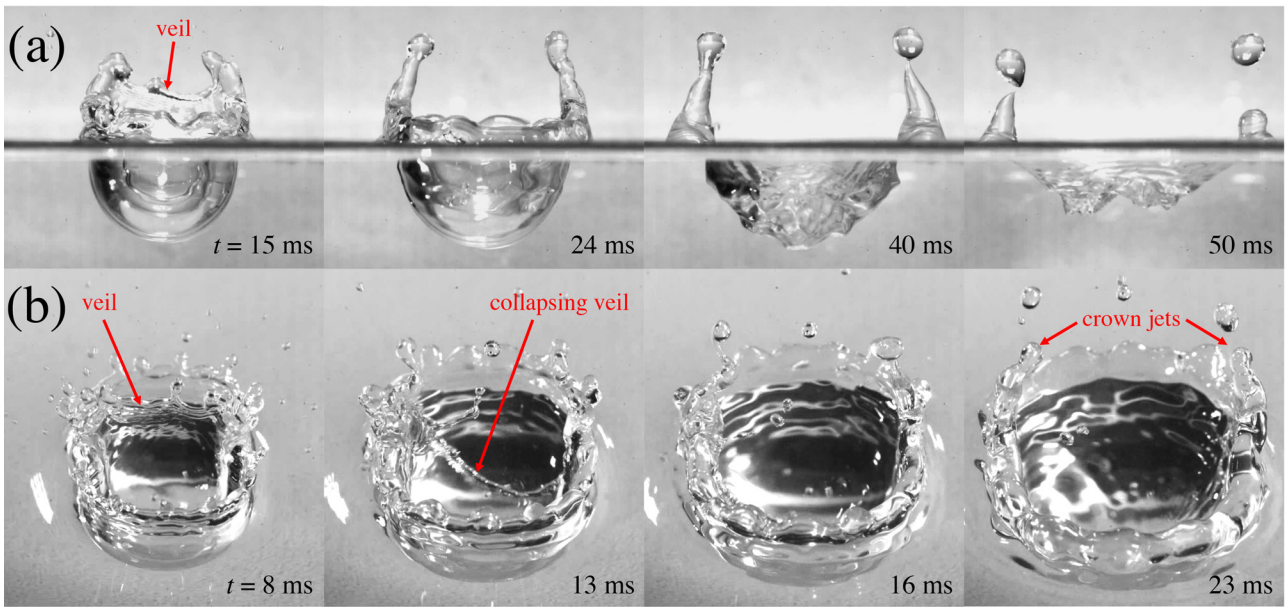

FIG. 8. The collapsing veil and formation of crown jets viewed from the side and (a) level with the free surface, and (b) looking down to the free surface. Case 7, Fr = 174. Multimedia view: https://doi.org/10.1063/5.0067442.4

initial conditions garnered from Eq. (5) such that $\alpha(2) = 1.11$, $\dot{\alpha}(2) = 0.17$, $\zeta(2) = -0.05$, and $\dot{\zeta}(2) = 0.36$.

We extract the minimum points of consecutive traces to obtain instantaneous measurements for dimensionless crater depths Γ, and employ the smoothing method of Epps *et al.*[30] by using a cubic spline within a critical error tolerance $\epsilon_{cr} = 1.3 \times 10^{-3}$ to approximate the true curves of Γ for all impact cases. Analysis of both temporal depth curves of Figs. 9(a)–9(c) confirms the reduction of U at drop impact. In keeping with the experimentally derived results of Bisighini *et al.*,[10] we consider a drop "penetration velocity" of $0.44U$ in our model and obtain reasonable approximations, $\lesssim 2\%$ difference for the maximum values of Γ across all cases with respect to single drop impacts. Our results thus compare well with the existing literature[10] on penetration mechanics, which show the velocity of penetration of the drop/target interface is approximately half of the impact velocity U. For $\tau < 2$, measurements conform to theoretical predictions to reflect the linearity of drop deformation in the initial phase of impact.[10] Thereafter ($\tau > 2$), crater expansion is governed by flow inertia where larger impact velocities U result in deeper craters. We however observe that the constriction of fluid flow for proximal cases 1, 4, and 7 results in shallower craters when compared to their single drop counterparts. The constants given in Eq. (5) could be adjusted to better mimic the experimental single drop curve (green) in Fig. 9(c), but we have chosen to employ identical values of $\dot{\alpha}$ and $\dot{\zeta}$ for all cases. The cause of deviation of case 7 from the theoretical prediction is unknown, but not unprecedented.[10]

C. Merging craters increase single crater stored energy

The drops' kinetic energy at impact, $E_k = mU^2/2$ where m is drop mass, is primarily converted for crater formation through a nearly inviscid process[10,31] and contributes to both gravitational potential energy and capillary energy. The gravitational potential energy in the expanded crater[18] is given by

$$P \sim \frac{\pi}{2}\rho g(\Gamma D)^2\left(\frac{\lambda D}{2}\right)^2, \tag{6}$$

where ΓD is the maximum dimensional crater depth and λD is the corresponding crater width at the free surface. The capillary energy at the moment when the crater is deepest

$$C \sim \pi\sigma\Gamma\lambda D^2. \tag{7}$$

Submillimeter craters are restored primarily through capillary forces, and as craters grow, gravity forces dominate.[32] While crater dynamics are influenced by the prolate form and oscillation of impacting drops,[33–35] we take no measure of these effects as the goal of this study is to define the broad features of twin impacting drops.

We plot P and C vs the kinetic energy of a single impacting drop E_k in Figs. 10(a) and 10(b), respectively. For non-merging craters, we take the average crater depth and radius to determine P and C. For all cases, potential and capillary energies increase with impact velocity, though potential energy grows most rapidly. The merging craters of cases 1, 4, and 7 (filled points) produce P and C values that are considerably greater than other cases released from the same height—a single merged crater is larger than individual craters. For non-merging craters, drop separation has no notable effect on crater energy. For simplicity, we do not consider crater-dependent prefactors[18] for Eqs. (6) and (7), but use those of a cylinder, which results in P values that are greater than the incident kinetic energy. Thus, the true prefactor[36] to Eq. (6) is certainly < 1, likely close to 0.25. As kinetic energy is reduced, it is converted more evenly between potential and capillary energies, as shown by the ratio P/C in Fig. 10(c). For most of the

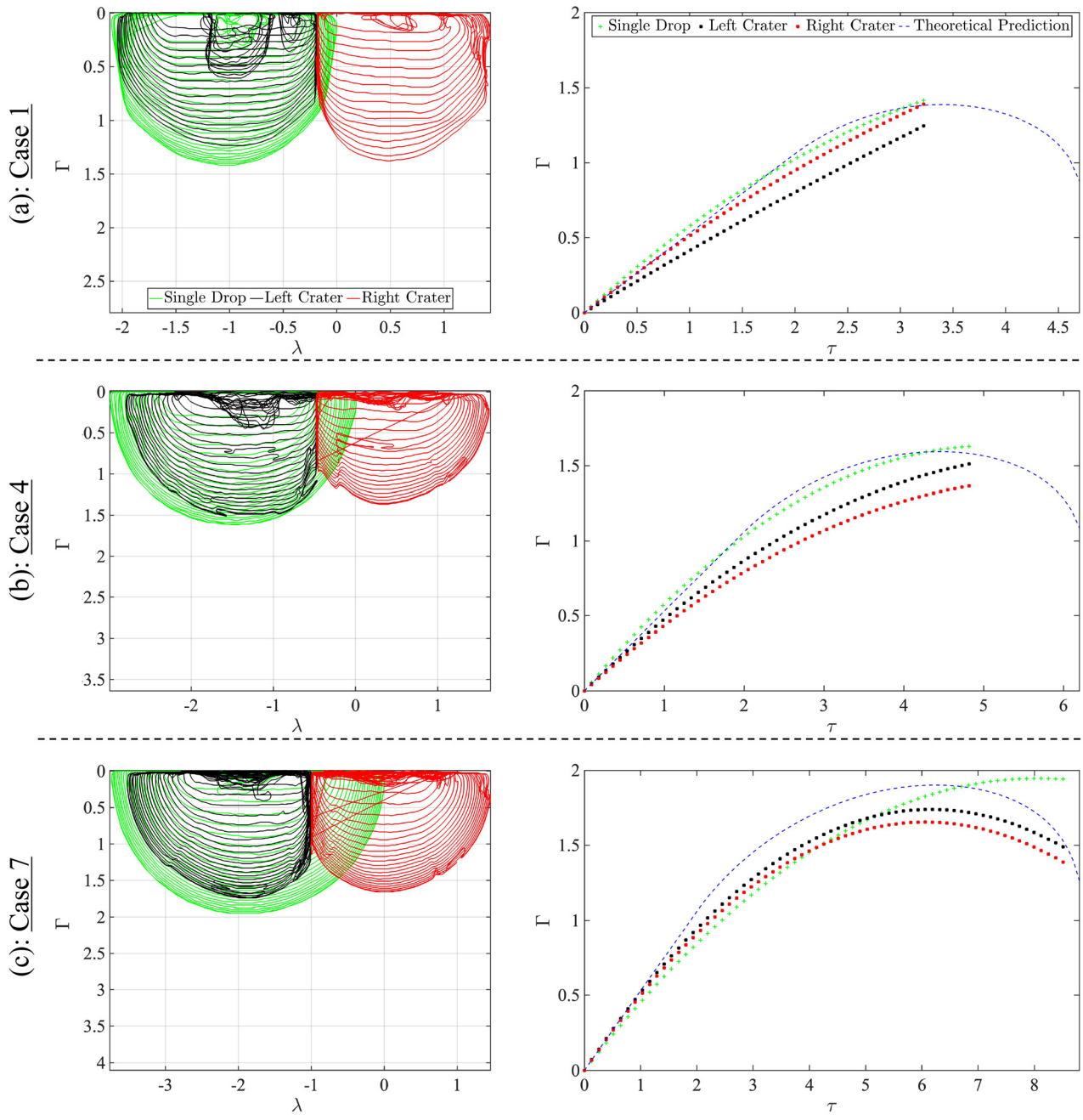

FIG. 9. Crater expansion for simultaneous drop impacts onto a deep liquid pool for drop separation $d = 5$ mm, where $\Gamma = y/D$, $\lambda = x/D$, and $\tau = Ut/D$. Plots correspond to cases (a) 1, (b) 4, and (c) 7. The legend in (a) applies to all panels. Twin drop impacts are compared with single drop impacts and theoretical predictions to elucidate the extent of drop separation on crater growth.

impacts considered here, stored crater energy is dominated by gravity, a domination more severe for merging craters.

The collapse of separate or merged craters produces supersurface jets. A theoretical treatment or physical scaling of jet height h_j does not exist in the literature to the authors' knowledge. We develop a scaling for jet height here using a similar approach to that developed for solid projectiles.[15] A hemispherical crater with depth ΓD and volume $\forall_{cr} \sim (\Gamma D)^3$ is subject to a buoyant force $F_b \sim \rho g \forall_{cr}$. The collapse of the crater is accompanied by boundary work $W_{cr} \sim F_b(\Gamma D)$, a process in which surface tension is negligible given that Bond

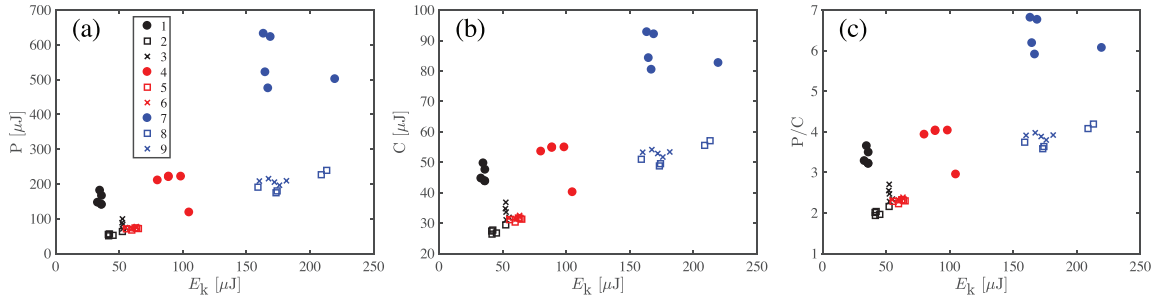

FIG. 10. Plots of (a) crater gravitational potential energy P, (b) crater capillary energy C, and (c) P/C vs single drop kinetic energy E_k. The legend in (a) applies to all panels.

number $\mathrm{Bo} = (\rho - \rho_a)g(\Gamma D)^2/\sigma = 6.2 \gg 1$, where $\rho_a = 1.2$ kg/m^3 is the density of air and using $\Gamma = 1.5$. The work of the collapsing crater is converted to gravitational potential energy in the jet, $F_b(\Gamma D) \sim \rho g \mathcal{V}_j h_j$, where $\mathcal{V}_j \sim D_j^2 h_j$ and D_j is jet diameter. Experience mandates that at our experimental scale the diameter of a disturbance of a free surface scales with the ensuing response,[15] $D_j \sim \Gamma D$. Thus, we may write $\rho g(\Gamma D)^4 \sim \rho g(\Gamma D)^2 h_j^2$, or simply

$$h_j/D \sim \Gamma. \tag{8}$$

Fitting Eq. (8) to our data in Fig. 11(a) produces a correlation coefficient $R^2 = 0.54$, while a best fit yields $h_j/D \sim \Gamma^{1.54}$ ($R^2 = 0.61$). The scatter in Fig. 11(a) is responsible for the small improvement in correlation coefficient with a significant change in the scaling coefficient. It should be noted that even with nearly perfect spherical impactors, jet height is quite variable in replicate tests.[15–17]

If the collapse of the crater is subject to boundary work W_{cr}, the expansion of the crater is subject to the same work, scaling with the kinetic energy of the falling drop, $\rho g \mathcal{V}_{cr}(\Gamma D) \sim \rho D^3 U^2$. Noting that $U^2 = (gD)\mathrm{Fr}$, we may write $\Gamma^4 \sim \mathrm{Fr}$ and when combined with Eq. (8),

$$h_j/D \sim \mathrm{Fr}^{1/4}. \tag{9}$$

Using all data, we find Eq. (9) gives a correlation coefficient $R^2 = 0.62$ and a best fit yields $h_j/D \sim \mathrm{Fr}^{0.35}$ ($R^2 = 0.68$). Although we use only a single drop to calculate Fr, we find the merging craters (filled circles) of cases 1, 4, and 7 fit well within the non-merging impacts. Merging imparts no advantage for creating higher jets as shown in Fig. 11(b). The cause is likely that merged craters are not distinctly deeper than their parents but are wider, which can be seen visually in Fig. 3 and is demonstrated by the crater dimensions plotted in Fig. 11(c).

IV. DISCUSSION

In this study, we present the emergence of unique splash phenomena when two drops impact a liquid pool simultaneously. The emergence of specific features within our defined cases has strong dependence on the velocity and spacing combinations of our drops. Arguably, we sample only a small portion of the available parameter space. An avenue for future research is increasing drop velocity and changing the viscosity of the drops and pool, both separately and together. Decreasing the Reynolds number at a constant Weber number alters crown morphology and suppresses its breakup.[37] Changes in crown dynamics will certainly change crown jet behavior, likely reducing crown jet height. The expression of crown jets and merging craters is very likely seen at drop separation distances well beyond 10 mm for larger, more energetic drops and for fluids with lower viscosity. Conversely, significant increases in viscosity are likely to stymie drop–drop interactions by reducing crater depth and suppressing supersurface features, thus providing a surrogate for lower impact energies. Support for this assertion is provided by the rightmost terms in Eqs. (3) and (4). An expansion of drop parameters, particularly toward velocities approaching terminal speeds, is an area for future work.

The theoretical predictions of crater evolution presented in Eqs. (3)–(5) present the ability to predict both crater expansion and retraction. It is worth noting that the efficacy of these equations at predicting

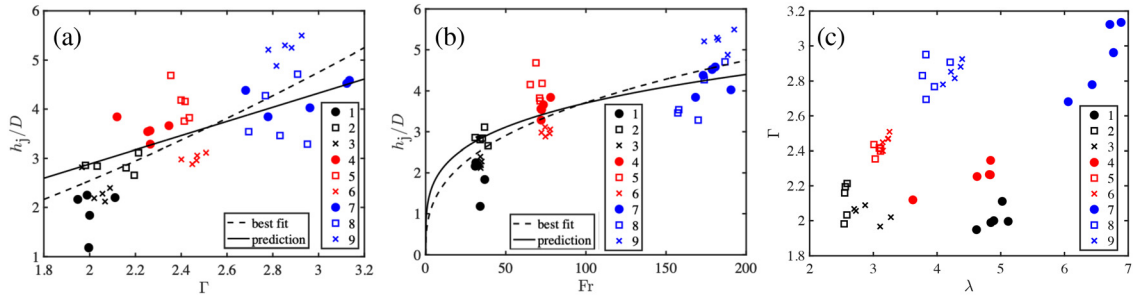

FIG. 11. Plots of (a) h_j/D vs non-dimensionalized crater depth Γ, (b) non-dimensionalized crater jet height above the free surface h_j/D vs Froude number, (c) non-dimensionalized crater depth Γ vs non-dimensionalized crater width λ.

retraction is marginal.[10] However, we believe it is possible for Eqs. (3)–(5) to nicely describe the retraction of a merged crater, but with adjusted constants. Furthermore, values of We, Fr, and Re will likewise need to be adjusted since the nature of the merged crater no longer resembles that of an individual, twin drop. The choice of these dimensionless groups for merged craters is not obvious. During the merging process, craters experience a dramatic increase in radius α and shift in centroid location ζ to lie above the free surface. The physics of crater merging are an area for future research.

With our system, it is not possible to reliably and cleanly release multiple drops along the axis of impact that produce the nested craters noted in previous works.[23,24] However, future researchers may choose to explore this line of inquiry. With sufficiently proximal impacts, we would expect nesting craters to interact with one another, to an extent. As craters become deeper in the fluid (second level and downward), hydrostatic pressure further restricts their size and thus their ability to push against one another.

ACKNOWLEDGMENTS

We would like to thank the National Science Foundation No. CBET-1941341, the University of Tennessee, the University of Central Florida, and Florida Polytechnic University for partial support.

DATA AVAILABILITY

Raw data were generated at the Open Science Framework: https://osf.io/v9gtf/ large-scale facility. Derived data supporting the findings of this study are available from the corresponding author upon reasonable request.

REFERENCES

[1]C. Josserand and S. T. Thoroddsen, "Drop impact on a solid surface," Annu. Rev. Fluid Mech. **48**, 365–391 (2016).
[2]A. P. Lebanoff and A. K. Dickerson, "Drop impact onto pine needle fibers with non-circular cross section," Phys. Fluids **32**, 092113 (2020).
[3]J. Lee, D. Derome, and J. Carmeliet, "Drop impact on natural porous stones," J. Colloid Interface Sci. **469**, 147–156 (2016).
[4]B. L. Scheller and D. W. Bousfield, "Newtonian drop impact with a solid surface," AIChE J. **41**, 1357–1367 (1995).
[5]A. Yarin, "Drop impact dynamics: Splashing, spreading, receding, bouncing…," Annu. Rev. Fluid Mech. **38**, 159–192 (2006).
[6]I. V. Roisman and C. Tropea, "Impact of a drop onto a wetted wall: Description of crown formation and propagation," J. Fluid Mech. **472**, 373 (2002).
[7]A. Prosperetti and H. N. Oguz, "The impact of drops on liquid surfaces and the underwater noise of rain," Annu. Rev. Fluid Mech. **25**, 577–602 (1993).
[8]D. W. Murphy, C. Li, V. d'Albignac, D. Morra, and J. Katz, "Splash behaviour and oily marine aerosol production by raindrops impacting oil slicks," J. Fluid Mech. **780**, 536–577 (2015).
[9]J. Breitenbach, I. V. Roisman, and C. Tropea, "From drop impact physics to spray cooling models: A critical review," Exp. Fluids **59**, 55 (2018).
[10]A. Bisighini, G. E. Cossali, C. Tropea, and I. V. Roisman, "Crater evolution after the impact of a drop onto a semi-infinite liquid target," Phys. Rev. E **82**, 036319 (2010).
[11]B. Ray, G. Biswas, and A. Sharma, "Regimes during liquid drop impact on a liquid pool," J. Fluid Mech. **768**, 492–523 (2015).
[12]S. T. Thoroddsen and K. Takehara, "The coalescence cascade of a drop," Phys. Fluids **12**, 1265–1267 (2000).
[13]S. L. Manzello, "An experimental study of a water droplet impinging on a liquid surface," Exp. Fluids **32**, 580 (2002).
[14]G. Agbaglah, M.-J. Thoraval, S. Thoroddsen, L. Zhang, K. Fezzaa, and R. Deegan, "Drop impact into a deep pool: Vortex shedding and jet formation," J. Fluid Mech. **764**, 1–12 (2015).
[15]D. A. Watson, C. J. Souchik, M. P. Weinberg, J. M. Bom, and A. K. Dickerson, "Making a splash with fabrics in hydrophilic sphere entry," J. Fluids Struct. **94**, 102907 (2020).
[16]D. A. Watson, J. L. Stephen, and A. K. Dickerson, "Jet amplification and cavity formation induced by penetrable fabrics in hydrophilic sphere entry," Phys. Fluids **30**, 082109 (2018).
[17]D. A. Watson, J. M. Bom, M. P. Weinberg, C. J. Souchik, and A. K. Dickerson, "Water entry dynamics of spheres with heterogeneous wetting properties," Phys. Rev. Fluids **6**, 044003 (2021).
[18]G.-J. Michon, C. Josserand, and T. Séon, "Jet dynamics post drop impact on a deep pool," Phys. Rev. Fluids **2**, 023601 (2017).
[19]Q. Deng, A. Anilkumar, and T. Wang, "The role of viscosity and surface tension in bubble entrapment during drop impact onto a deep liquid pool," J. Fluid Mech. **578**, 119 (2007).
[20]H. C. Pumphrey and P. A. Elmore, "The entrainment of bubbles by drop impacts," J. Fluid Mech. **220**, 539–567 (1990).
[21]D. Morton, M. Rudman, and L. Jong-Leng, "An investigation of the flow regimes resulting from splashing drops," Phys. Fluids **12**, 747–763 (2000).
[22]X. Qu, A. Goharzadeh, L. Khezzar, and A. Molki, "Experimental characterization of air-entrainment in a plunging jet," Exp. Therm. Fluid Sci. **44**, 51–61 (2013).
[23]N. B. Speirs, Z. Pan, J. Belden, and T. T. Truscott, "The water entry of multi-droplet streams and jets," J. Fluid Mech. **844**, 1084 (2018).
[24]R. Hurd, T. Fanning, Z. Pan, C. Mabey, K. Bodily, K. Hacking, N. Speirs, and T. Truscott, "Matryoshka cavity," Phys. Fluids **27**, 091104 (2015).
[25]X. Liu, Y. Qu, Y. Wang, M. Wang, Z. Wang, and H. Sun, "Numerical analysis of two hollow drops simultaneously impacting a wet surface," Phys. Fluids **33**, 043312 (2021).
[26]D. Henderson, W. Pritchard, and L. Smolka, "On the pinch-off of a pendant drop of viscous fluid," Phys. Fluids **9**, 3188 (1997).
[27]X. Wang and X. Lyu, "Experimental study on vertical water entry of twin spheres side-by-side," Ocean Eng. **221**, 108508 (2021).
[28]J. de Ruiter, R. E. Pepper, and H. A. Stone, "Thickness of the rim of an expanding lamella near the splash threshold," Phys. Fluids **22**, 022104 (2010).
[29]M. M. Mansoor, J. O. Marston, I. U. Vakarelski, and S. T. Thoroddsen, "Water entry without surface seal: Extended cavity formation," J. Fluid Mech. **743**, 295–326 (2014).
[30]B. P. Epps, T. T. Truscott, and A. H. Techet, "Evaluating derivatives of experimental data using smoothing splines," in *Proceedings of Mathematical Methods in Engineering International Symposium* (MMEI, Lisbon, Portugal, 2010), pp. 29–38.
[31]H. N. Oguz and A. Prosperetti, "Bubble entrainment by the impact of drops on liquid surfaces," J. Fluid Mech. **219**, 143–179 (1990).
[32]E. Ghabache, A. Antkowiak, C. Josserand, and T. Séon, "On the physics of fizziness: How bubble bursting controls droplets ejection," Phys. Fluids **26**, 121701 (2014).
[33]M.-J. Thoraval, Y. Li, and S. T. Thoroddsen, "Vortex-ring-induced large bubble entrainment during drop impact," Phys. Rev. E **93**, 033128 (2016).
[34]A.-B. Wang, C.-C. Kuan, and P.-H. Tsai, "Do we understand the bubble formation by a single drop impacting upon liquid surface?," Phys. Fluids **25**, 101702 (2013).
[35]S. Thoroddsen, T. Etoh, K. Takehara, N. Ootsuka, and Y. Hatsuki, "The air bubble entrapped under a drop impacting on a solid surface," J. Fluid Mech. **545**, 203 (2005).
[36]L. J. Leng, "Splash formation by spherical drops," J. Fluid Mech. **427**, 73 (2001).
[37]D. R. Guildenbecher, C. F. Brooks, and P. E. Sojka, "Viscous drops impacting thin liquid surfaces: Experimental quantification of secondary fragment size and velocities," Technical Report No. 2891C (Sandia National Laboratory (SNL-NM), Albuquerque, New Mexico, 2015).